Mech. Sci., 5, 37–52, 2014
www.mech-sci.net/5/37/2014/
doi:10.5194/ms-5-37-2014

Mechanical Sciences
Open Access

Segmental contributions to the ground reaction force in the single support phase of gait

D. S. Mohan Varma and S. Sujatha

Department of Mechanical Engineering, Indian Institute of Technology Madras, Chennai, India

Correspondence to: S. Sujatha (sujsree@iitm.ac.in)

Received: 2 May 2014 – Revised: 10 July 2014 – Accepted: 24 July 2014 – Published: 19 August 2014

Abstract. An inverse dynamics model for the single support (SS) phase of gait is developed to study segmental contributions to the ground reaction force (GRF). With segmental orientations as the generalized degrees of freedom (DOF), the acceleration of the body's center-of-mass is expressed analytically as the summation of the weighted kinematics of individual segments. The weighting functions are constants that are functions of the segment masses and center-of-mass distances. Using kinematic and anthropometric data from literature as inputs, and using the roll-over-shape (ROS) to model the foot-ground interaction, GRF obtained from the inverse model are compared with measured GRF data from literature. The choice of the generalized coordinates and mathematical form of the model provides a means to weigh individual segment contributions, simplify models and choose more kinetically accurate inverse dynamics models. For the kinematic data used, an anthropomorphic model that includes the frontal plane rotation of the pelvis in addition to the sagittal DOF of the thigh and shank most accurately captures the vertical component of the GRF in the SS phase of walking. Of the two ROS used, the ankle-foot roll-over shape provides a better approximation of the kinetics in the SS phase. The method presented here can be used with additional experimental studies to confirm these results.

1 Introduction

In inverse dynamics models of gait, measured kinematics, estimated body segment parameters (BSP) and measured ground reaction force (GRF) are usually used as inputs to compute the internal joint forces and moments (Winter, 2005). GRF are external forces acting on the body, and introducing them as inputs in the inverse model overdetermines the problem (Hatze, 1981). This overdeterminacy results in a residual error in the joint kinetics computations (Riemer et al., 2008). In this work, an inverse dynamics model that uses only the kinematics and BSP as inputs is developed. The measured GRF is used to validate the model.

The motivation for this work is a mathematical model that can be extended to study asymmetric gait with only kinematic measurements as inputs. This model for normal walking can serve as a baseline model for asymmetric gait, such as the gait of a prosthesis user, since errors in the anthropomorphic model are accounted for.

Mathematical models of gait vary from simple planar link-segment models (Onyshko and Winter, 1980; Winter, 2005; Mochon and McMahon, 1980) to complex musculoskeletal models (Anderson and Pandy, 2001). A simplified model for gait cannot capture all the characteristics of human walking, while a complex model becomes analytically intractable. Ideally, a mathematical model for gait should include all the degrees of freedom (DOF) that are major contributors to the activity. Six quantities, namely, the rotation of pelvis in the frontal and transverse planes, knee flexion in the stance phase, rotations of the foot and knee and the lateral movement of the pelvis were identified as the six determinants of gait (Saunders et al., 1953). Although, the influence of these DOF on the vertical center-of-mass (COM) motion and energy cost has been debated (Kuo, 2007), it is accepted that these six quantities are characteristic features of gait. The individual contributions of these and possibly other DOF to the overall kinetics needs to be quantified. By knowing the DOF that are active contributors, one can determine the kinematics that must be most accurately measured and reduce or add DOF to the mathematical model to make it simpler or more accurate.

Various researchers have used forward or inverse models to predict the GRF. Pandy and Berme (1989b) used a three-dimensional forward dynamics model that used five of the six determinants of gait for the simulation of normal gait to quantify the influence of individual gait determinants on the GRF and studied (Pandy and Berme, 1989a) the compensatory actions required when each of these DOF was systematically removed from the model. The model used was not an anthropomorphic model, and the joint moments were heuristically selected. Mochon and McMahon (1980) used a ballistic model for the swing phase, which assumed zero moments at the joints, to study the influence of the determinants of gait on the GRF. Thornton-Trump and Daher (1975) obtained GRF and joint kinetics from an inverse model and used these data as inputs for the analysis of a polycentric prosthetic knee. Zarrugh (1981) obtained GRF from an inverse model to study joint powers but did not include a pelvis link. Winiarski and Rutkowska-Kucharska (2009) used inverse dynamics to study the suitability of estimating GRF from the kinematics of the COM in normal and pathological gait. Pillet et al. (2010) obtained GRF from an inverse model for a force-plate-less estimation of center of pressure (COP) trajectory during gait. Oh et al. (2013) used an artificial neural networks-based analysis for force-plate-less estimation of GRF.

While forward dynamic models require joint moments (which cannot be measured directly) to be specified; inverse dynamics models need kinematic data as inputs. The general trends of joint/segment angles in normal gait have been studied extensively and are readily available in the literature (Saunders et al., 1953; Inman et al., 1981; Perry, 1992). Therefore, an inverse dynamics model that incorporates all the sagittal plane DOF of the lower limb segments, the frontal and transverse plane rotation of the pelvis, lateral movement of the legs and a single head-arms-and-trunk (HAT) segment is developed in this work. Newton's equation is rewritten to express GRF as a weighted summation of segmental kinematics. This enables the study of contributions of each of the DOF/segment kinematics to the GRF in a more direct way. Expressing the model in terms of contributions of individual segments will enable extension of the model to study asymmetric gait, such as the gait of a prosthesis user, where the properties and kinematics of the prosthetic limb are likely to differ from those of the unaffected side.

Many inverse dynamics models suffer from errors in kinematics (noise in measurements, errors due to data filtering, curve fitting technique used and derivative computation) and BSP (mass, inertia and COM location) estimates. While some studies (Pàmies-Vilà et al., 2012; Reinbolt et al., 2007) suggest that errors in kinematic data influence joint moment estimates more than the errors in BSP estimates, others (Rao et al., 2006; Pearsall and Costigan, 1999) show that the influence of BSP errors cannot be neglected. In all the above cases, the sensitivity of the joint reactions to the perturbations in the kinematics and BSP are studied using the overdetermined inverse model. Since joint reactions cannot be measured experimentally, the validity of these studies is dependent on the accuracy of the model. In this work, comparison of the GRF from the model to the measured values provides a means to determine the accuracy of the model, and the use of segmental orientations as the generalized DOF enables us to obtain analytical expressions for the contributions of each segment's kinematics to the GRF results. By systematically eliminating the DOF whose contribution is not significant, an optimal number of measurements needed for a reasonable estimation of GRF can be obtained. This can reduce the number of kinematic measurements and BSP estimates and thereby reduce the corresponding errors.

Apart from kinematics and BSP, the COP and foot kinematics (Mccaw and Devitat, 1995; Silva and Ambrosio, 2004) have also been found to influence the joint moment computations. Simulation studies on gait have used models such as the triple rocker (Perry, 1992), polynomial fits (Ju and Mansour, 1988; Ren et al., 2007) and COP-based fits (Koopman et al., 1995; Srinivasan et al., 2008). McGeer (1990) used circular arcs for the plantar surface of the foot in passive dynamic walkers, and Vanderpool et al. (2008) found that rolling feet are energetically efficient and can account for the loss of ankle motion. In their experimental studies, Hansen et al. (2004) define foot roll-over shape (FROS) and ankle-foot roll-over shape (AFROS) based on COP data. Their experimental studies found that the AFROS remains the same irrespective of changes in walking speed (Hansen et al., 2004), heel height (Hansen and Childress, 2004) and load carriage (Hansen and Childress, 2005). They also found that a person controls the ankle kinematics to maintain a consistent ROS (Wang and Hansen, 2010) and that in the case of a trans-tibial prosthesis user, an alignment for better walking performance for a given type of prosthetic foot can be determined using this ROS (Hansen et al., 2000). Srinivasan et al. (2009) used Hansen's ROS in a forward dynamics model for the gait of trans-tibial prosthesis users. Since the FROS and AFROS shapes are backed by extensive experimental studies, we use these models to model the foot-ground interface in our work.

Optimization is used in this work to ensure that the input data satisfies the kinematic constraint of the swing foot clearing the ground during the SS phase. Unlike other optimization-based inverse models (Koopman et al., 1995; Ren et al., 2007) in which optimization is used in parallel with the inverse model to predict the kinematics, kinetics or both, here optimization is used only to correct any errors in data that cause violation of the kinematic constraints. The effects of using the FROS and AFROS (Hansen et al., 2004) models on the GRF computations are studied.

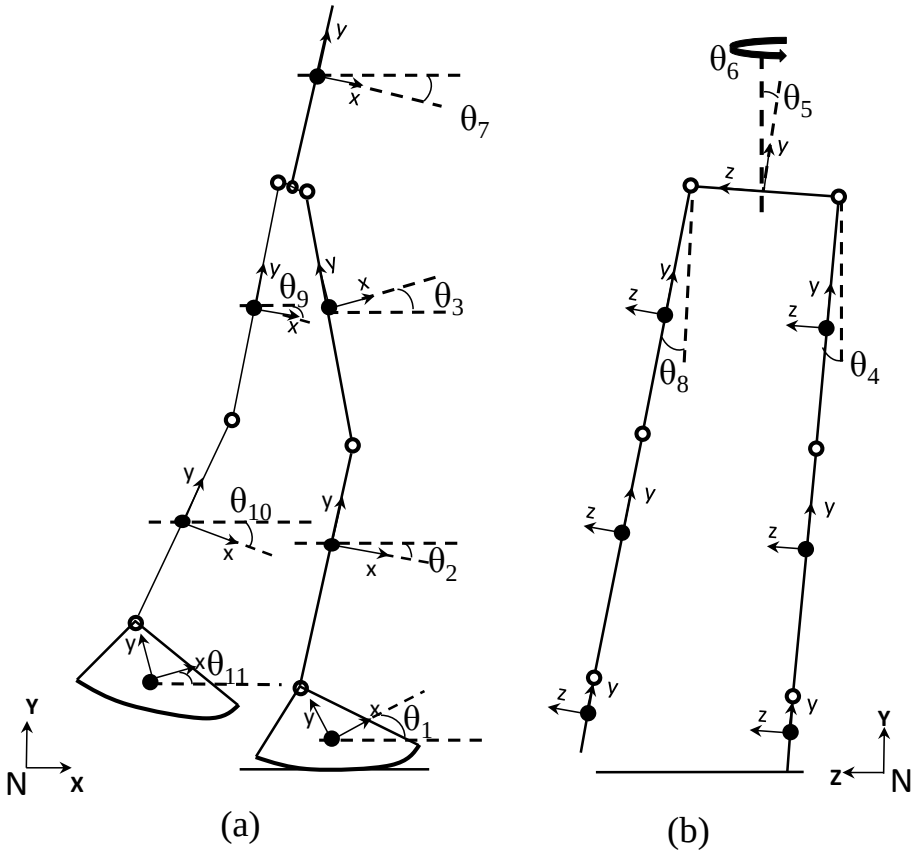

Figure 1. Stick figures showing the angles in the **(a)** sagittal and **(b)** frontal planes. All angles are measured with respect to N. (HAT segment is not shown in the frontal plane **b**.)

2 Methods

2.1 Mathematical model

The anthropomorphic model of gait consists of eight segments and eleven DOF (Fig. 1). The eight segments are: the foot, shank and thigh of each leg, the pelvis and the HAT. The segments of the leg – foot, shank and thigh – are assumed to remain in the same plane and are connected by revolute joints at the hip, knee and ankle. Transverse plane rotation of the leg is assumed to be zero. Thus, the stance leg has 4 DOF: sagittal plane rotations of the foot (θ_1), shank (θ_2) and thigh (θ_3) and the frontal plane rotation of the leg as a whole (θ_4). The swing leg also has 4 DOF – sagittal plane rotations of the foot (θ_{11}), shank (θ_{10}) and thigh (θ_9) and the frontal plane rotation of the leg as a whole (θ_8). The pelvis has two DOF – rotation in the frontal(θ_5) and transverse planes (θ_6). The HAT segment is assumed to be rotating only in the sagittal plane (θ_7). The angles in the frontal, transverse and sagittal planes are measured as the orientation of the body-fixed x, y or z axis with respect to the ground-fixed X, Y and Z axes respectively. The body-fixed coordinate systems of the segments are as shown in Fig. 1. The pelvis is modeled as a massless link, and the HAT segment is assumed to be connected to the mid-point of the pelvis. The foot-ground interaction is modeled using two different foot models:

1. A rolling contact foot model with Hansen's Foot ROS (Fig. 2).
2. A rolling contact foot model using Hansen's Ankle-Foot ROS (Fig. 3).

The FROS is obtained by transforming the COP data from N (the coordinate system fixed to the ground) to a coordinate system fixed to the foot at the ankle, and the AFROS is obtained by transforming the COP data from N to a coordinate system fixed to the shank at the ankle. In the latter case, the AFROS takes into account ankle flexion and models the net motion as rolling motion of the shank and foot complex with respect to the ground so that the ankles of the swing and stance legs can be assumed to be rigid in the mathematical model. The angles of the foot segment θ_1 and θ_{11} are then determined using $\theta_1 = \theta_2 - \theta_{\text{ank}}$ and $\theta_{11} = \theta_{10} - \theta_{\text{ank}}$. The value θ_{ank} is the angle between the shank and the foot segments that remains constant since the AFROS accounts for the ankle flexion. Therefore, while the model using the FROS has eleven DOF, the model using AFROS has only nine DOF.

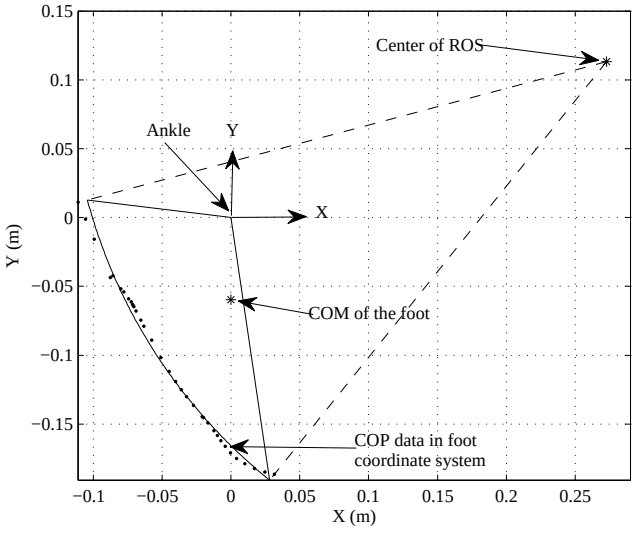

Figure 2. FROS with y axis (of the coordinate system fixed to the foot) lying along the line joining the ankle and the COM of the foot.

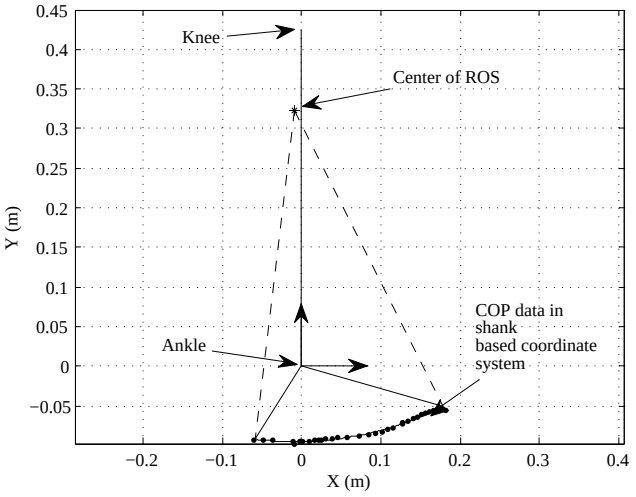

Figure 3. AFROS with y axis (of the coordinate system fixed to the shank) along the shank length.

2.2 Kinematics

The position, velocity and acceleration (in N) of a point BP on a rigid body B moving in space with respect to another point BQ on the same body (expressed in N) are given by

$$\begin{aligned}
&\boldsymbol{P}_{\mathrm{BP/BQ}}=\boldsymbol{P}_{\mathrm{BP}}-\boldsymbol{P}_{\mathrm{BQ}}=\mathbf{T}_{\mathrm{B}}\boldsymbol{r}^{\mathrm{B}},\\
&\boldsymbol{V}_{\mathrm{BP/BQ}}=\boldsymbol{V}_{\mathrm{BP}}-\boldsymbol{V}_{\mathrm{BQ}}=\boldsymbol{\omega}_{\mathrm{B}}\times\mathbf{T}_{\mathrm{B}}\boldsymbol{r}^{\mathrm{B}} \text{ and}\\
&\boldsymbol{A}_{\mathrm{BP/BQ}}=\boldsymbol{A}_{\mathrm{BP}}-\boldsymbol{A}_{\mathrm{BQ}}=\boldsymbol{\alpha}_{\mathrm{B}}\times\mathbf{T}_{\mathrm{B}}\boldsymbol{r}^{\mathrm{B}}+\boldsymbol{\omega}_{\mathrm{B}}\times\left(\boldsymbol{\omega}_{\mathrm{B}}\times\mathbf{T}_{\mathrm{B}}\boldsymbol{r}^{\mathrm{B}}\right)
\end{aligned} \tag{1}$$

respectively, where $\boldsymbol{\alpha}_{\mathrm{B}}$ is the angular acceleration, $\boldsymbol{\omega}_{\mathrm{B}}$ is the angular velocity of body B in N (expressed in N), $\mathbf{T}_{\mathrm{B}}$ is the 3×3 transformation matrix obtained using space-fixed Z-Y-X transformations (Kane et al., 1983) and $\boldsymbol{r}^{\mathrm{B}}$ is the position vector from point BQ to BP expressed in B.

The above equations can be rewritten as

$$\begin{aligned}
&\boldsymbol{P}_{\mathrm{BP/BQ}}=\mathbf{T}_{\mathrm{B}}\boldsymbol{r}^{\mathrm{B}},\\
&\boldsymbol{V}_{\mathrm{BP/BQ}}=\mathbf{C}_{\mathrm{B}}\boldsymbol{r}^{\mathrm{B}} \text{ and}\\
&\boldsymbol{A}_{\mathrm{BP/BQ}}=\mathbf{E}_{\mathrm{B}}\boldsymbol{r}^{\mathrm{B}}
\end{aligned} \tag{2}$$

where $\boldsymbol{C}_{\mathrm{B}}=\tilde{\omega}_{\mathrm{B}}\mathbf{T}_{\mathrm{B}}$, $\mathbf{E}_{\mathrm{B}}=\tilde{\alpha}_{\mathrm{B}}\mathbf{T}_{\mathrm{B}}+\tilde{\omega}_{\mathrm{B}}\mathbf{C}_{\mathrm{B}}$ and the skew-symmetric matrix $\tilde{\mathbf{q}}$ of any general vector $\boldsymbol{q}=(q_x,\,q_y,\,q_z)'$ is given as (Shabana, 2010)

$$\tilde{\mathbf{q}}=\begin{bmatrix} 0 & -q_z & q_y\\ q_z & 0 & -q_x\\ -q_y & q_x & 0 \end{bmatrix}. \tag{3}$$

The product $\mathbf{E}_{\mathrm{B}}\boldsymbol{r}^{\mathrm{B}}$ of Eq. (2) can also be written in column vector notation as

$$\mathbf{E}_{\mathrm{B}}\boldsymbol{r}^{\mathrm{B}}=r_x^{\mathrm{B}}\begin{bmatrix}|\\ \mathbf{E}_{\mathrm{B}}\\ |\end{bmatrix}_{c1}+r_y^{\mathrm{B}}\begin{bmatrix}|\\ \mathbf{E}_{\mathrm{B}}\\ |\end{bmatrix}_{c2}+r_z^{\mathrm{B}}\begin{bmatrix}|\\ \mathbf{E}_{\mathrm{B}}\\ |\end{bmatrix}_{c3} \tag{4}$$

where the subscripts $c1$, $c2$ and $c3$ indicate the first, second and third columns of the matrix $\mathbf{E}_{\mathrm{B}}$, respectively. Using the above notation, the acceleration of the COM can be expressed as (Appendix A)

$$\boldsymbol{A}_{\mathrm{com}}={}^{\mathrm{st}}\boldsymbol{A}_{\mathrm{ank}}+\sum k\begin{bmatrix}|\\ \mathbf{E}\\ |\end{bmatrix} \tag{5}$$

where ${}^{\mathrm{st}}\boldsymbol{A}_{\mathrm{ank}}$ is the acceleration of the ankle of the stance leg, ks are functions of mass fractions and COM distances and $\mathbf{E}$s are dependent on the kinematics of the segments.

2.3 Segmental contributions to GRF

Newton's equation of motion for the whole body in the SS phase is given by

$$\boldsymbol{GRF}=M\boldsymbol{A}_{\mathrm{com}}-M\boldsymbol{g}=M\left(\boldsymbol{A}_{\mathrm{com}}-\sum m_i\boldsymbol{g}\right)=\sum\boldsymbol{R}_i \tag{6}$$

where m_i is the mass fraction of the ith segment, M is the total mass and $\boldsymbol{g}$ is the gravity vector. Expressing all the accelerations in terms of $\mathbf{E}$s, GRF can be rewritten as the summation of contributions from each segment's kinematics as (Appendix A)

$$\begin{aligned}
\boldsymbol{GRF}=&{}^{\mathrm{st}}\boldsymbol{R}_{\mathrm{ft}}+{}^{\mathrm{st}}\boldsymbol{R}_{\mathrm{sk}}+{}^{\mathrm{st}}\boldsymbol{R}_{\mathrm{th}}+\boldsymbol{R}_{\mathrm{pel}}\\
&+\boldsymbol{R}_{\mathrm{hat}}+{}^{\mathrm{sw}}\boldsymbol{R}_{\mathrm{th}}+{}^{\mathrm{sw}}\boldsymbol{R}_{\mathrm{sk}}+{}^{\mathrm{sw}}\boldsymbol{R}_{\mathrm{ft}}
\end{aligned} \tag{7}$$

where $\boldsymbol{R}_i$s are the segmental contributions and the superscripts "sw" and "st" indicate swing leg and stance leg, respectively, and the subscripts "ank", "ft", "sk", "th", "hat" and "pel" indicate the ankle, foot, shank, thigh, HAT and pelvis segments, respectively. The contributions of the segmental kinematics towards the GRF are given by Eqs. (A8) to (A15). The segmental contribution $\boldsymbol{R}_i$ has units of force.

Each of the $\boldsymbol{R}_i$s is expressed as a summation of a variable acceleration term ($M\,k_i\,\mathbf{E}_i$) and a constant gravity term ($m_i\,M\,\boldsymbol{g}$). The k_is in the acceleration terms are functions of the mass fractions of multiple segments and the distance of the COM from the joints (Eq. A5), and each $\mathbf{E}_i$ is a function of the kinematics of segment i. For a given set of anthropometric data (estimated segment masses and COM distances), each $\boldsymbol{R}_i$ is a function of only the kinematics of a particular segment. The foot segment's contribution ${}^{\mathrm{st}}\boldsymbol{R}_{\mathrm{ft}}$ is also dependent on the ankle acceleration (${}^{\mathrm{st}}\boldsymbol{A}_{\mathrm{ank}}$), which is determined by the ROS used (Appendix B). Using the anthropometric data from Winter (2005) in Eq. (A5), we get (in m) $k_1 = -0.0009$, $k_2 = 0.41$, $k_3 = 0.28$, $k_4 = 0.144$, $k_5 = 0.194$, $k_6 = -0.033$, $k_7 = -0.0147$ and $k_8 = -0.0009$.

The segmental contributions to the vertical component of GRF (GRFy) are given by (y components in Eqs. A8 to A15)

$$
\begin{aligned}
&{}^{\mathrm{st}}R_{\mathrm{fty}} = M\,{}^{\mathrm{st}}A_{\mathrm{anky}} + Mk_1\left(-S_1\alpha_1 - \left(\omega_4^2+\omega_1^2\right)C_1C_4\right.\\
&\left.-\alpha_4S_4C_1\right) + {}^{\mathrm{st}}m_{\mathrm{ft}}Mg,\\
&{}^{\mathrm{st}}R_{\mathrm{sky}} = Mk_2\left(-S_2\alpha_2 - \left(\omega_4^2+\omega_2^2\right)C_2C_4 - \alpha_4S_4C_2\right)\\
&+ {}^{\mathrm{st}}m_{\mathrm{sk}}Mg,\\
&{}^{\mathrm{st}}R_{\mathrm{thy}} = Mk_3\left(-S_3\alpha_3 - \left(\omega_4^2+\omega_3^2\right)C_3C_4 - \alpha_4S_4C_3\right)\\
&+ {}^{\mathrm{st}}m_{\mathrm{th}}Mg,\\
&R_{\mathrm{pely}} = Mk_4\left(\omega_5\omega_6S_6 + \omega_5^2S_5C_6 - \alpha_5C_5C_6\right),\\
&R_{\mathrm{haty}} = Mk_5\left(-S_7\alpha_7 - \omega_7^2C_7\right) + m_{\mathrm{hat}}Mg,\\
&{}^{\mathrm{sw}}R_{\mathrm{thy}} = Mk_6\left(-S_9\alpha_9 - \left(\omega_8^2+\omega_9^2\right)C_9C_8 - \alpha_8S_8C_9\right)\\
&+ {}^{\mathrm{sw}}m_{\mathrm{th}}Mg,\\
&{}^{\mathrm{sw}}R_{\mathrm{sky}} = Mk_7\left(-S_{10}\alpha_{10} - \left(\omega_8^2+\omega_{10}^2\right)C_{10}C_8 - \alpha_8S_8C_{10}\right)\\
&+ {}^{\mathrm{sw}}m_{\mathrm{sk}}Mg \text{ and}\\
&{}^{\mathrm{sw}}R_{\mathrm{fty}} = Mk_8\left(-S_{11}\alpha_{11} - \left(\omega_8^2+\omega_{11}^2\right)C_{11}C_8 - \alpha_8S_8C_{11}\right)\\
&+ {}^{\mathrm{sw}}m_{\mathrm{ft}}Mg
\end{aligned}
\tag{8}
$$

where, $S_i = \sin\theta_i$, $C_i = \cos\theta_i$, $\omega_i = \dot{\theta}_i$, $\alpha_i = \ddot{\theta}_i$, M is the total mass and ${}^{\mathrm{st}}A_{\mathrm{anky}}$ is the vertical component of the acceleration of the ankle of the stance leg given by Eq. (B1). The segmental contributions to the anterior-posterior component of GRF (GRFx) and medio-lateral component of GRF (GRFz) can also be obtained from Eqs. (A8) to (A15).

Each segmental contribution is a function of one or two DOF. To study the contribution of a DOF of a particular segment, the other DOF is set equal to zero. For instance, the contributions of pelvis to GRFx and GRFy are given by,

$$
\begin{aligned}
R_{\mathrm{pel}x} &= Mk_4\left(-\omega_6^2S_6 - \omega_5\omega_6S_5C_6 + \alpha_6C_5C_6\right)\\
R_{\mathrm{pely}} &= Mk_4\left(\omega_5\omega_6S_6 + \omega_5^2S_5C_6 - \alpha_5C_5C_6\right).
\end{aligned}
\tag{9}
$$

When θ_5, ω_5 and α_5 are set equal to zero, the contributions of transverse plane rotation of the pelvis (θ_6) are given by,

$$
\begin{aligned}
R_{\mathrm{pel}x} &= Mk_4\left(-\omega_6^2S_6 + \alpha_6C_6\right)\\
R_{\mathrm{pely}} &= 0
\end{aligned}
\tag{10}
$$

and when θ_6, ω_6 and α_6 are set equal to zero, the contributions of frontal plane rotation of the pelvis (θ_5) are given by,

$$
\begin{aligned}
R_{\mathrm{pel}x} &= 0\\
R_{\mathrm{pely}} &= Mk_4\left(\omega_5^2S_5 - \alpha_5C_5\right).
\end{aligned}
\tag{11}
$$

The above equations show that the transverse plane rotation of the pelvis has no effect on the GRFy and the frontal plane rotation has no effect on the GRFx.

2.4 Unknown kinematics

The kinematic data from Winter (2005) are used to study the segmental contributions to the GRF. The sagittal plane rotations of the foot, shank, thigh and HAT are obtained from Winter (2005). The frontal plane rotation of the leg (θ_4 and θ_8) is assumed based on general gait trends in normal gait (Inman et al., 1981; Perry, 1992). In normal gait, the trajectory of any point on the pelvis, including the hip joints, in the transverse plane is a sine curve (Inman et al., 1981). Therefore, the trajectory in the transverse plane of any point on the pelvis can be given by $Z = C\,\sin(\omega t + \phi)$, where $\omega = 2\pi/T$ and T is the period of the gait cycle. The maximum lateral translation of the pelvis is approximately 0.02 m and is reached slightly after mid-stance (Inman et al., 1981). Using these two assumptions, the values of C and ϕ were determined. The height above the ground of the hip joint is known from the hip trajectory data (Winter, 2005), while the equation for Z gives the amount of lateral displacement. Using this information, the frontal plane rotation of the leg is determined for the entire stance phase. A Fourier series curve for the full gait cycle is fit using this data to determine the leg angle in the frontal plane during swing.

Using the available data and the fact that gait is symmetric for a normal person, the frontal plane rotation (θ_5) and the transverse plane rotation (θ_6) of the pelvis are obtained as follows: from the hip trajectory data (Winter, 2005), it is seen that the height above the ground (y coordinate) of the hip joint at ipsilateral and contralateral heel contact (HC) is approximately the same. This equality implies that in symmetric gait (as is the case here) at HC the height above the ground of the right and left hips is the same, indicating that the pelvis is level with (i.e. parallel to) the ground in the frontal plane at HC. Also, Inman et al. (1981) reported gait characteristics of six adult males walking at moderate walking speed and found that, in general, the pelvis is level with the ground in the frontal plane at HC. Therefore, the pelvis rotation in the frontal plane (θ_5) at HC is assumed to be zero.

From the hip trajectory data, the hip displacement in the direction of progression (x direction) from ipsilateral HC to contralateral HC (say d_1) and the hip displacement in the direction of progression from contralateral HC to ipsilateral HC (say d_2) are known. Again, due to the symmetry of normal gait, the distance along the x direction between the right and left hips at right HC ($x_1 - x_2$) must be the same as that at left HC $(x_2 + d_2) - (x_1 + d_1)$. Since d_1 and d_2 are known quantities, this equality can be solved to obtain $\delta x = x_1 - x_2$. This value δx, in turn can be used to obtain the transverse plane angular position (θ_6) of the pelvis at HC. For the kinematic data from Winter (2005), the value of θ_6 at HC is 10.3°.

Since the relative position of the hips at HC is known, a unit vector along the line joining the hip joints, $\boldsymbol{h}$, at HC is known. Using the sagittal plane hip trajectory data from Winter (2005) and Z, the 3-D trajectories of the right and left hips, and therefore the vector $\boldsymbol{h}$, are known for the full gait cycle. For a Z-Y-X transformation with no rotation about the Z axis, the DOF θ_5 and θ_6 can be computed using

$$\theta_5 = \text{atan}\left(-h_y / h_z\right) \text{ and}$$
$$\theta_6 = \text{atan}\left(-h_x S_5 / h_y\right). \quad (12)$$

Fourier series curves are fit to all the kinematic data (θ_1 through θ_{11}). In order to determine the number of Fourier coefficients n required for each fit, the least squares errors are determined as n is increased. For each of the fits, the n (as it is increased) that results in a change in the least squares error that is less than one degree is chosen. In order to ensure symmetry of the gait data, the time period used for the Fourier series fit for the HAT segment is half that of the others, and only odd harmonics of the Fourier series are used for the pelvis DOF.

2.5 Optimization

In the single support phase of walking the stance leg is in contact with the ground while the swing leg clears the ground as it moves forward. In experimentally obtained kinematic data, due to errors, the data may indicate that the swing leg contacts or digs into the ground. This is a violation of the kinematic constraint that the swing leg remains above the ground in the SS phase. To address this issue, in this work, optimization is used to modify the segment angles such that the swing leg remains above the ground during SS phase. No kinetic constraints or energy criteria are employed, and the optimization merely serves to render the kinematics realistic. With the input kinematic data and FROS, the kinematic constraints are not violated. However, when AFROS is used, the constraints are violated in the swing phase just before HC. The optimization problem statement for this case is given as

$$\begin{aligned} &\text{Minimize} \quad |\boldsymbol{x} - \boldsymbol{x}_0| \\ &\text{such that,} \quad y_{\min} \geq \Delta \\ &\boldsymbol{x} - \delta\boldsymbol{x} \leq \boldsymbol{x} \leq \boldsymbol{x} + \delta\boldsymbol{x} \end{aligned} \quad (13)$$

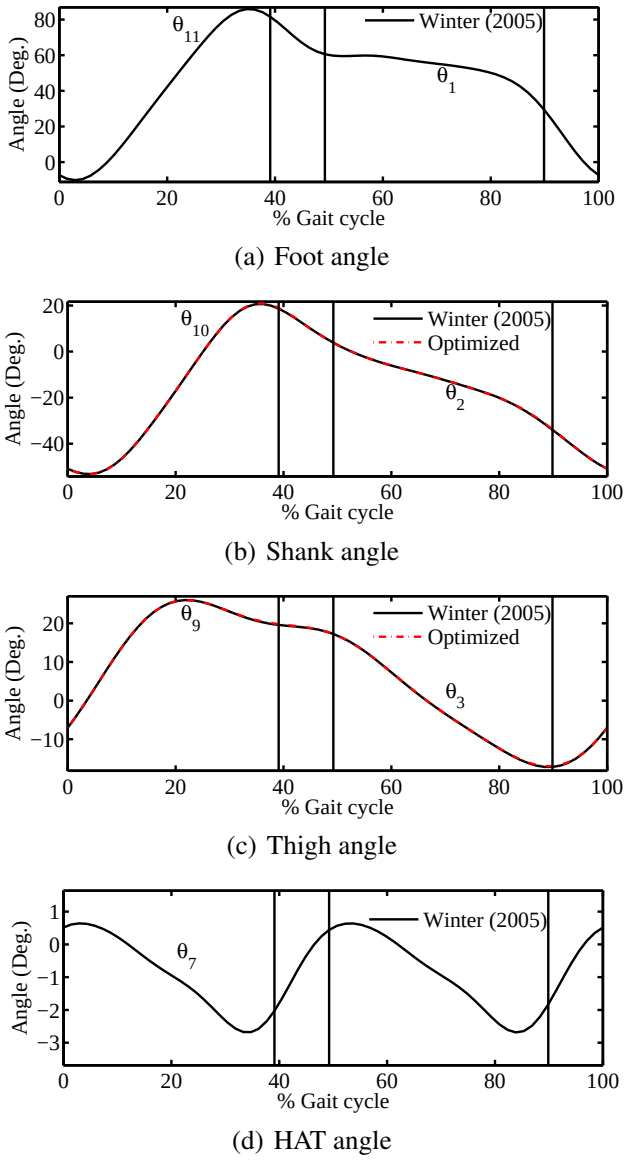

(a) Foot angle

(b) Shank angle

(c) Thigh angle

(d) HAT angle

Figure 4. Sagittal plane kinematic data for full gait cycle (toe-off to toe-off) (Winter, 2005). **(a)** Foot, **(b)** shank, **(c)** thigh and **(d)** HAT angles. For **(a)**–**(c)** the data from 0 to 39 % gait cycle indicate data for the swing leg and angles from 50 to 89 % gait cycle indicate data for the stance leg in the SS phase.

where $\boldsymbol{x}$ is the vector $[\theta_2, \theta_3, \theta_4, \theta_5, \theta_6, \theta_8, \theta_9, \theta_{10}]$ and $y_{\min}$ is the y coordinate of the lowest point on the foot. To ensure minimal deviation from known trends, small values of 1° and 1 mm are chosen for $\delta\boldsymbol{x}$ and Δ, respectively. Every instance of the SS phase is checked for constraint violation, and optimization is performed whenever there is a violation. Fourier series curves are fit again to the optimized kinematic data. The optimization and curve fitting are thus performed iteratively until a set of kinematics that satisfies the constraints are obtained. It can be seen from Figs. 4 and 5 that after optimization, the kinematic data show little or no variation from

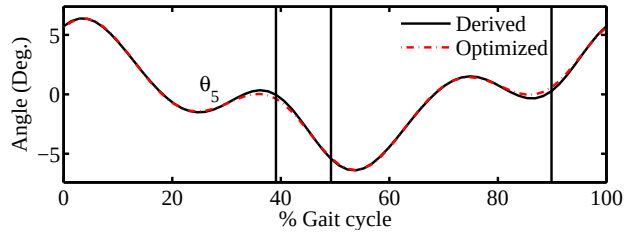

(a) Pelvis angle in frontal plane

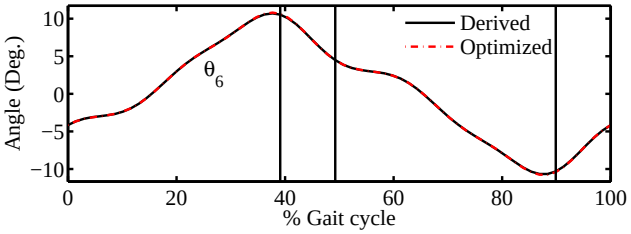

(b) Pelvis angle in transverse plane

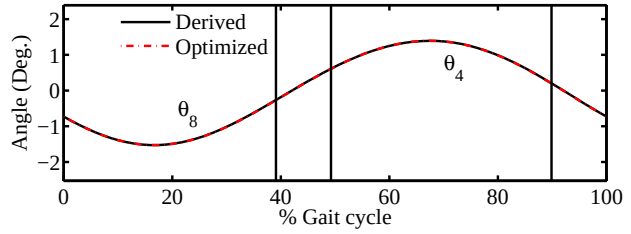

(c) Leg angle in the frontal plane

Figure 5. Derived frontal plane and transverse plane kinematic data for full gait cycle (toe-off to toe-off). Pelvis angles **(a, b)** in the frontal and transverse planes and leg angle **(c)** in the frontal plane. For **(c)** data from 0 to 39 % gait cycle indicate data for the swing leg and data from 50 to 89 % gait cycle indicate data for the stance leg in the SS phase.

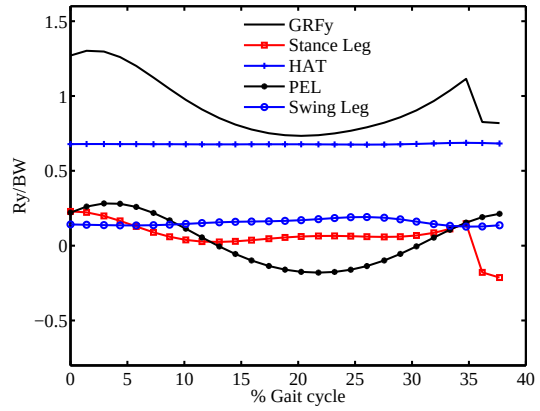

(a)

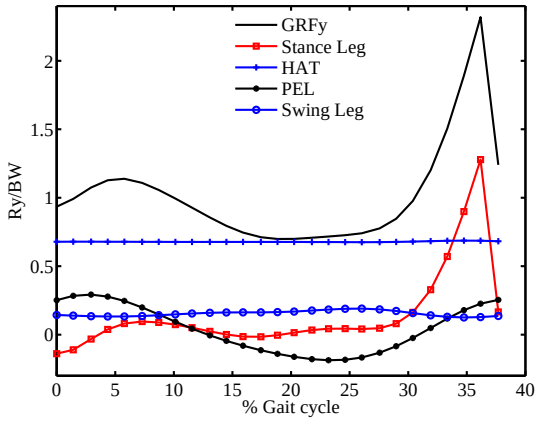

(b)

Figure 6. GRFy and stance leg, HAT, pelvis and swing leg contributions during SS phase as a fraction of body weight with **(a)** AFROS and **(b)** FROS. (Gait cycle starts at toe-off of the other leg, that is, at the beginning of SS.)

the initial data except for pelvis rotation in the frontal plane (Fig. 5a) around HC of right leg (39 % of gait cycle). Once a valid set of kinematics are obtained, these data are used to study the contribution of kinematics to the GRF.

3 Results

The segmental contributions of the stance leg (foot, shank and thigh), pelvis, swing leg and HAT (expressed as a fraction of body weight – BW) to GRFy and GRFx from the models using AFROS and FROS are shown in Figs. 6 and 7, respectively. Between the models using AFROS and FROS, the contributions of the stance leg segments showed variation (Fig. 8) while the contributions from the segments of the swing leg remained similar as expected. The contributions of the segments of the swing leg to GRFy for the model that uses AFROS are shown in Fig. 9. The variations in the swing leg contributions to GRFy are much smaller, and the contributions are almost constant compared to the contributions of the stance leg and pelvis (Fig. 6). The contributions of the HAT to GRFy are also relatively constant (Fig. 6). The variable acceleration terms ($k_i \mathbf{E}_i$s) of $\boldsymbol{R}_i$ of the swing leg segments (Eqs. A13 to A15) are rendered negligible by the small values of the corresponding k_is. In the case of the HAT segment, the $k_i \mathbf{E}_i$ of the contribution (Eq. A12) is small due to minimal change in the HAT angle (Fig. 4d, HAT angle has a range of 4°). Hence, only the segment weights (that is, the gravity terms in Eqs. A12 to A15) of the HAT and swing leg segments contribute to GRFy. The difference between RMS values (Table 1) with all the DOF and without the DOF of the swing leg and HAT is approximately 0.01 BW for GRFy. This difference is negligible given that the GRFy varies around 1 BW in the SS phase of normal walking. Therefore, the DOFs of the swing leg and HAT, θ_7 to θ_{11}, can be eliminated from the equation for GRFy.

The contribution of the transverse plane rotation of the pelvis to GRFy (Eq. 10, Fig. 10) is zero, and the contribution of the frontal plane rotation of the pelvis to GRFy (Eq. 11, Fig. 10) is the same as when both the DOF are included. In

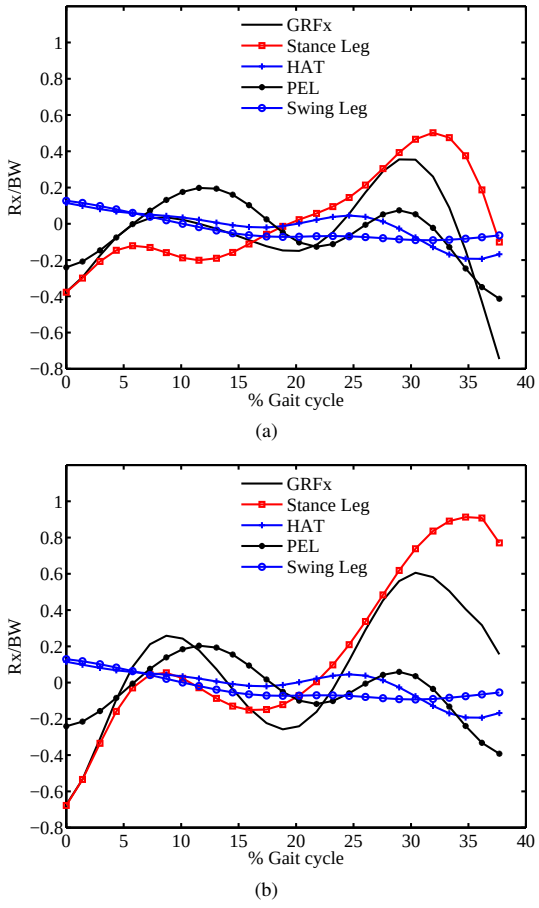

Figure 7. GRFx and stance leg, HAT, pelvis and swing leg contributions to GRFx during SS phase as a fraction of body weight with **(a)** AFROS and **(b)** FROS. (Gait cycle starts at toe-off of the other leg, that is, at the beginning of SS.)

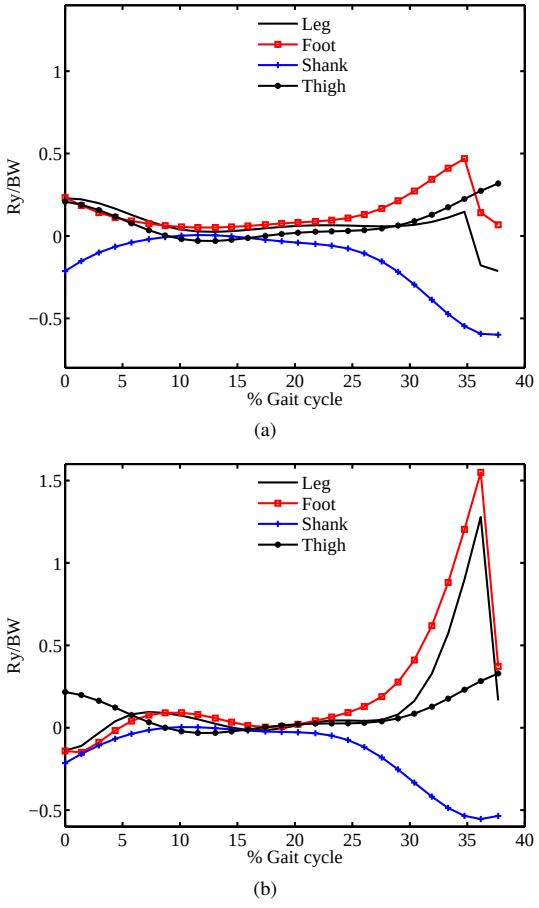

Figure 8. Contributions from foot, shank and thigh of the stance leg and sum of all three (Leg) to GRFy in SS phase as a fraction of body weight with **(a)** AFROS and **(b)** FROS models for the foot. (Gait cycle starts at toe-off of the other leg, that is, at the beginning of SS.)

other words, the entire contribution from the pelvis segment to GRFy comes from the frontal plane rotation θ_5. The RMS values also show a minimal change in GRFy (Table 1) when θ_6 is ignored, while the difference is considerable when θ_5 is ignored. Also, the contribution of the frontal plane rotation of the stance leg to GRFy (Fig. 11) is almost zero (no difference in the RMS value with all DOF and when $\theta_4 = 0$ in Table 1), confirming the dominance of the sagittal plane DOF of the leg. Therefore, the measurement of θ_4 and θ_6 is not required for the computation of GRFy.

In the case of GRFx, the pelvis and the stance leg are the most dominant contributors (Fig. 7). The contributions of the swing leg and HAT, however, are not constant as in the case of GRFy. Moreover, the GRFx obtained from the models gave an RMS error of 0.25 and 0.28 BW for AFROS and FROS, respectively, and the results showed a poor match with the experimental data (Fig. 13).

4 Discussion

4.1 Reduced model for GRFy

Most mathematical models include only sagittal plane kinematics (Selles et al., 2001; Ren et al., 2007; Martin and Schmiedeler, 2014) and avoid the pelvis link. Mochon and McMahon (1980) use a ballistic swing phase model but do not include the frontal plane rotation of the pelvis or ankle plantarflexion in their model. Their results for GRFy do not show the characteristic double hump, and they concluded that frontal plane rotation of the pelvis is probably necessary to capture that. Our result confirms that conclusion and shows that the frontal plane rotation of the pelvis is a major contributor to the characteristic shape of GRFy and must be included in a mathematical model for gait. One contradictory result is from Pandy and Berme (1989b) who, in their forward dynamics simulation, found that the pelvic list (frontal plane rotation of the pelvis) is not a dominant dynamical determinant of GRFy. However, their model was not anthropomorphic

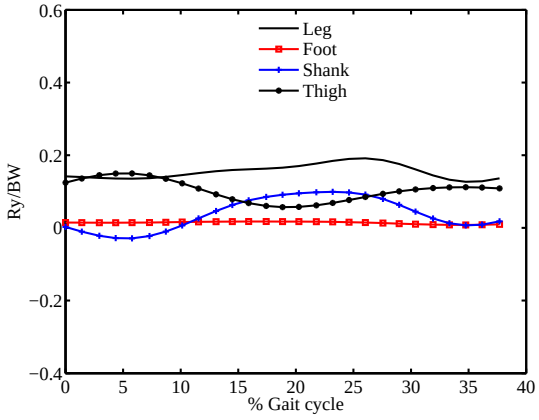

Figure 9. Contributions from foot, shank and thigh of the swing leg and sum of all three (Leg) to GRFy is SS phase as a fraction of body weight with AFROS.The results from the model with FROS are similar. (Gait cycle starts at toe-off of the other leg, that is, at the beginning of SS.)

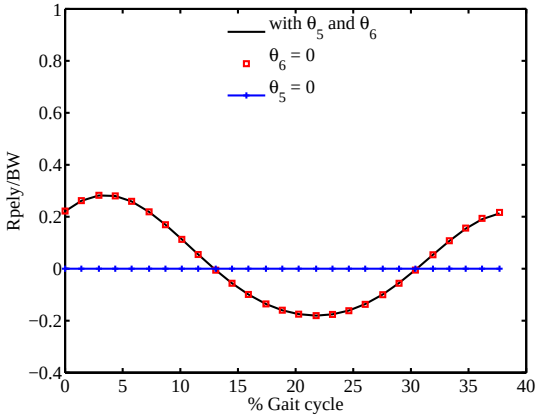

Figure 10. Contributions of pelvis DOF – θ_5 and θ_6 to GRFy in SS phase expressed as a fraction of body weight with AFROS. The results from the model with FROS are similar. (Gait cycle starts at toe-off of the other leg, that is, at the beginning of SS.)

because they neglected the effect of the foot and attached a massless damped spring between the hip and ankle of the stance leg.

The results of the segmental contributions showed that the sagittal plane DOFs of the stance leg and the frontal plane rotation of the pelvis link are the most dominant DOFs for the prediction of GRFy. Based on these observations, the analytical expression for GRFy in SS phase of gait can be reduced to

$$\begin{aligned}\mathrm{GRFy} \approx\ & Mg + Ms_x\left(\alpha_1 C_1 - \omega_1^2 S_1\right) \\ & + M\left(k_1 + s_y\right)\left(-\alpha_1 S_1 - \omega_1^2 C_1\right) \\ & + Mk_2\left(-S_2\alpha_2 - \omega_2^2 C_2\right) + Mk_3\left(-S_3\alpha_3 - \omega_3^2 C_3\right) \\ & + Mk_4\left(\omega_5^2 S_5 - \alpha_5 C_5\right). \end{aligned} \quad (14)$$

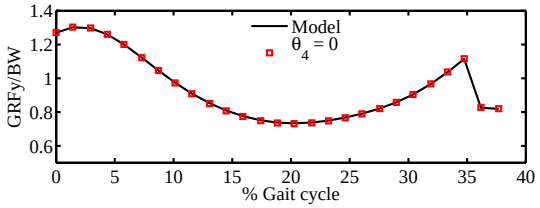

Figure 11. GRFy results for SS phase with all DOF and without the frontal plane rotation of the leg ($\theta_4 = 0$) with AFROS. The results from the model using FROS are similar. (Gait cycle starts at toe-off of the other leg, that is, at the beginning of SS.)

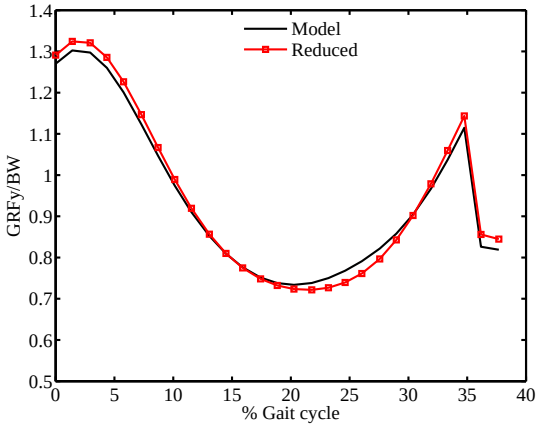

Figure 12. GRFy results when all the DOFs are used and with minimal DOFs in the model with AFROS. The results for the model using FROS are similar. (Gait cycle starts at toe-off of the other leg, that is, at the beginning of SS.)

When FROS is used for the foot-ground interface, the GRFy estimation requires measurement of four DOF (θ_1, θ_2, θ_3 and θ_5). When AFROS is used, the number of required DOF is reduced to three since $\theta_1 = \theta_2 - \theta_{\mathrm{ank}}$, $\omega_1 = \omega_2$ and $\alpha_1 = \alpha_2$. The GRFy estimated using minimal kinematics match closely with the GRFy from the model with all the DOFs (Fig. 12). The RMS error between GRFy from the model with all DOF and with minimal kinematics are 0.0202 BW for FROS and 0.0198 BW for AFROS. Therefore, measurement of sagittal plane kinematics of the stance leg and the frontal plane rotation of the pelvis is sufficient to obtain a good approximation of GRFy.

4.2 GRFx for inverse dynamics analysis

The GRFx obtained from the model cannot be used in an inverse dynamics model as this would give large errors in the horizontal joint forces and joint moments. Research (Herr and Popovic, 2008) shows that the angular momentum regulation in gait influences the horizontal component of GRF. Koopman et al. (1995) ensured that the kinematics are such that the GRF vector passes though the COM and obtained GRFx and GRFz that matched well with the experimental

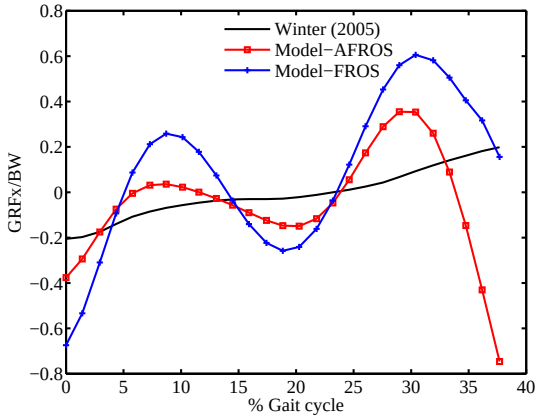

Figure 13. GRFx results for SS phase – experimental data and results using AFROS and FROS foot models. (Gait cycle starts at toe-off of the other leg, that is, at the beginning of SS.)

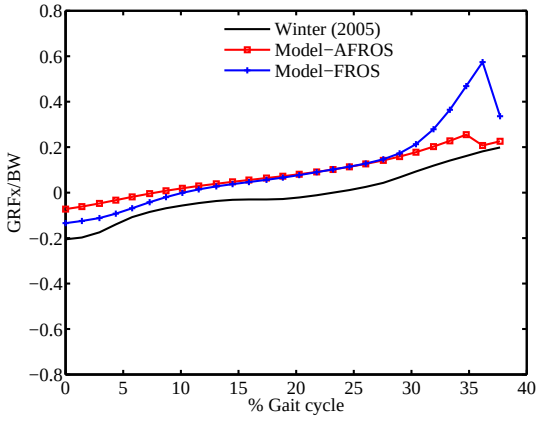

Figure 14. GRFx results for SS phase – experimental data and results for AFROS and FROS foot models using GRFy and the assumption that the GRF vector passes through the COM. (Gait cycle starts at toe-off of the other leg, that is, at the beginning of SS.)

data. Making this assumption, the GRFx at every instance is computed as

$$\mathrm{GRFx} = \left(u_x/u_y\right)\mathrm{GRFy} \tag{15}$$

where $\boldsymbol{u}$ is the vector from the contact point to the COM. The GRFx obtained using this assumption (Fig. 14) show a better match with the experimental data than the GRFx obtained from the model (Fig. 13). The GRFx obtained using this assumption gave an RMS error of 0.09BW and 0.13BW for AFROS and FROS models, respectively.

4.3 Foot roll over shapes

The input kinematic data for both the models are similar, and hence, the segmental contributions for all the segments showed similar patterns (Figs. 6 and 7) except for the contributions from the stance foot (Fig. 8). This discrepancy can

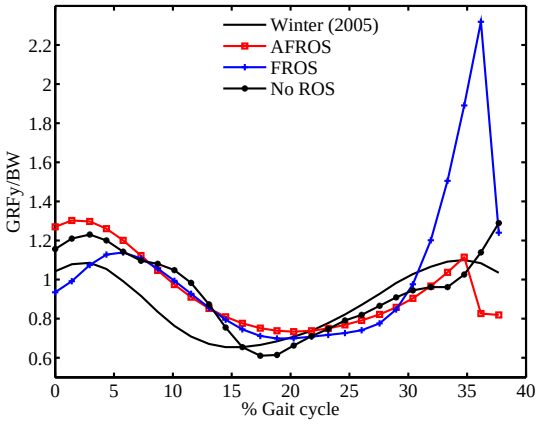

Figure 15. GRFy results for SS phase – experimental data (Winter, 2005) and results using rolling foot models and without using any ROS model. (Gait cycle starts at toe-off of the other leg, that is, at the beginning of SS.)

be attributed to the ROS models used. From Eq. (A6), we observe that the ankle acceleration has a direct correlation to GRF while the rest of the kinematics (**E**s) are scaled by a factor less than one. Therefore, the accuracy with which the foot model predicts the acceleration of the ankle joint plays a significant role in accurate GRF computation. The GRFy obtained using the FROS model reaches a very high value towards the end of the SS phase when compared to GRFy when the AFROS model was used (Fig. 15). This difference could be due to the fact that the ankle is assumed to be rigid for AFROS model but not for the FROS model. The circular ROS takes into account the plantarflexion of the ankle joint, and since the FROS model has both rolling motion and ankle plantarflexion, the combined effect has likely resulted in overprediction of GRFy towards the end of the SS phase (Fig. 15).

In order to understand the effect of using a ROS, the GRF is computed using the ankle acceleration directly from Winter (2005). In other words, the ${}^{\mathrm{st}}\boldsymbol{A}_{\mathrm{ank}}$ in Eq. (A6) is obtained directly from experimental data as opposed to the models with ROS in which case the ${}^{\mathrm{st}}\boldsymbol{A}_{\mathrm{ank}}$ is computed using Eq. (B1). In all three cases, there is a consistent overprediction of GRFy in the first half of the SS phase (Fig. 15). When FROS is used, the first peak of the GRFy curve is shifted forward, while the model with AFROS gives a peak at approximately the same % gait cycle as the experimental values. Even in the case where no ROS is used, the GRFy curve does not match the experimental values well (RMS error = 0.1399 BW), possibly due to measurement errors. The RMS error for GRFy is lower in the case where no ROS is used (0.1399 BW) when compared to RMS error when the FROS and AFROS models are used for the foot-ground interaction (Table 1). This result shows that direct measurement of the ankle kinematics is better than using a model for the foot. However, using a ROS to model the foot-ground

Table 1. RMS values of predicted GRFy (normalized by BW) with respect to the experimental values.

GRFy	All DOF	θ_7 to $\theta_{11} = 0$	$\theta_6 = 0$	$\theta_5 = 0$	$\theta_4 = 0$	Reduced model θ_4, θ_6 and θ_7 to $\theta_{11} = 0$
AFROS	0.1571	0.1664	0.1570	0.1777	0.1567	0.1660
FROS	0.3195	0.3308	0.3204	0.2840	0.3198	0.3322

interaction would enable comparison of a prosthetic foot to a normal foot or comparisons involving different prosthetic feet and varying alignments without collecting gait data each time. Since the purpose of this study is to extend the model to the analysis of the gait of a prosthesis user, the two ROS models are compared.

Both the FROS and AFROS are derived using the same COPx data. Although the ROS captures the geometric shape of the rolling foot, the dynamics associated with the FROS and AFROS are different, resulting in changes in the corresponding GRFy. In other words, the ROS models the displacement of the foot with respect to the ground more accurately than it models the time derivatives of the displacement. The discrepancy is less pronounced in the case of the AFROS model. The RMS error for GRFy from the two models (0.1571 BW with AFROS foot model and 0.3195 BW with FROS model in Table 1) show that the AFROS gives a better approximation than the FROS.

While the model's ability to accurately predict the timing of the first peak is sensitive to the foot model used (which in turn is dependent on the COP trajectory), multiple factors could be influencing the overprediction in the first half of the SS phase. The contribution from the HAT segment to GRFy is essentially constant and is dependent on its estimated mass. Any change in the HAT segment's estimated mass would increase or decrease the magnitude of GRFy without changing the shape of the peak. Also, the head, arms and trunk are modeled as a single segment. A model that includes more segments (that is, more DOFs) in the upper body could improve the results. All the segments are assumed to be rigid, and the overprediction could be due to the lack of compliance in the model. The use of a damped spring attached to the segments of the stance leg as in Pandy and Berme (1988) to account for the damping in the leg could potentially improve the GRF results.

5 Conclusions

The choice of segmental orientations with respect to a ground reference frame as the generalized DOF enables the expression of the GRF vector as a linear combination of the columns of segmental kinematics (**E** matrices). This mathematical form enables the study of the influence of the kinematics of a chosen segment or DOF, resulting in a reduced model for GRFy.

Results from this work show that the pelvic rotation in the frontal plane, the rolling foot model and the sagittal plane rotations of the segments of the stance leg are the major contributors to GRFy in the SS phase of gait. Of the two ROS, the AFROS provides a better approximation of GRFy. A minimal 3-DOF (rotations of the thigh and shank in the sagittal plane, and pelvic rotation in the frontal plane) anthropomorphic model can be used to approximate GRFy. Using the reduced model can enable gait studies in settings other than a gait lab by using minimal kinematic measurements and predetermined ROS characteristics (radius, arc length and center of ROS location) of the foot (Hansen et al., 2000).

A systematic reduction of the mathematical model to obtain a simplistic yet effective model is possible if a complete set of 3-D kinematic data and BSP are available. In this work, due to the lack of a full set of kinematic data, the frontal plane rotation of the legs was assumed, and the pelvis DOF were derived using the hip trajectory in the sagittal plane and the fact that gait is symmetric. However, this is not a limitation of the modeling procedure itself. While the lack of full data limited the validation of the model to the one set of gait data (Winter, 2005), the typical patterns of the joint angles and the GRF for normal walking are well-established (Inman et al., 1981; Perry, 1992; Srinivasan et al., 2008), which lends confidence to the model's validity.

A limitation of the model is the inaccuracy in predicting the GRFx directly from the model. Balance considerations, however, are known to play a role in influencing GRFx (Herr and Popovic, 2008; Firmani and Park, 2013). Using the GRFy from the reduced model with the assumption of angular momentum control for balance better approximates the GRFx, indicating that this condition is necessary for the model to be useful for inverse dynamic analysis.

Even though this work does not perfectly model normal gait, its usefulness is as a baseline for asymmetric gait. The form of the model enables easy extension to model asymmetric gait where the BSP and kinematics of the segments of the right and left sides vary, as in the case of prosthesis users. The use of ROS enables the analysis of the gait of prosthesis users with different prosthetic feet since experimental data for ROS of different prosthetic feet have been reported (Hansen et al., 2000, 2004; Hansen and Childress, 2004). The radius of the ROS and the center-of-ROS location are representative of the compliance and the alignment of the prosthetic limb, respectively (Hansen et al., 2000; Srinivasan et al., 2009). The effect of different prosthetic feet (modeled

by different ROS), alignments and mass distributions of the prosthetic limb, etc., can be studied. The results can be compared using the developed normal gait model as the baseline model. This comparison would be more appropriate than comparison of a model for asymmetric gait to experimental normal gait data since the baseline model accounts for errors due to modeling assumptions.

The methodology described can be used with more sets of experimental data to determine statistically the minimum DOFs and ideal ROS for the model. The developed model can be extended to the double support (DS) phase by incorporating additional kinematic constraints in the optimization since some of the DOF will be dependent as a result of the closed loop kinematic chain formed by the limb segments in DS. Modeling DS would also require assumptions on the load sharing between the two legs (Ren et al., 2007; Koopman et al., 1995). Future work will include the study of the double support phase and sensitivity of joint moments and forces to perturbations in the kinematic data such as in the case of the gait of prosthesis users.

Appendix A: Derivation of analytical expressions for segmental contributions

The position vectors $\boldsymbol{r}_2$ through $\boldsymbol{r}_{14}$ (Fig. A1) expressed in the respective body-fixed coordinate systems are given by-

$$\begin{aligned}
&\boldsymbol{r}_2 = [0\, r_{2y}\, 0]', \ \boldsymbol{r}_3 = [0\, r_{3y}\, 0]', \ \boldsymbol{r}_4 = [0\, r_{4y}\, 0]',\\
&\boldsymbol{r}_5 = [0\, r_{5y}\, 0]', \ \boldsymbol{r}_6 = [0\, r_{6y}\, 0]', \ \boldsymbol{r}_7 = [0\, r_{7z}\, 0]',\\
&\boldsymbol{r}_8 = [0\, r_{8y}\, 0]', \ \boldsymbol{r}_9 = [0\, r_{9z}\, 0]', \ \boldsymbol{r}_{10} = [0\, r_{10y}\, 0]',\\
&\boldsymbol{r}_{11} = [0\, r_{11y}\, 0]', \ \boldsymbol{r}_{12} = [0\, r_{12y}\, 0]', \ \boldsymbol{r}_{13} = [0\, r_{13y}\, 0]' \text{ and}\\
&\boldsymbol{r}_{14} = [0\, r_{14y}\, 0]'. \qquad \text{(A1)}
\end{aligned}$$

The acceleration of the COM $\boldsymbol{A}_{\text{com}}$ can be written as

$$\begin{aligned}
\boldsymbol{A}_{\text{com}} =& {}^{\text{st}}m_{\text{ft}}\, {}^{\text{st}}\boldsymbol{A}_{\text{ft}} + {}^{\text{st}}m_{\text{sk}}\, {}^{\text{st}}\boldsymbol{A}_{\text{sk}} + {}^{\text{st}}m_{\text{th}}\, {}^{\text{st}}\boldsymbol{A}_{\text{th}}\\
&+ m_{\text{pel}}\boldsymbol{A}_{\text{pel}} + m_{\text{hat}}\boldsymbol{A}_{\text{hat}}\\
&+ {}^{\text{sw}}m_{\text{th}}\, {}^{\text{sw}}\boldsymbol{A}_{\text{th}} + {}^{\text{sw}}m_{\text{sk}}\, {}^{\text{sw}}\boldsymbol{A}_{\text{sk}} + {}^{\text{sw}}m_{\text{ft}}\, {}^{\text{sw}}\boldsymbol{A}_{\text{ft}} \qquad \text{(A2)}
\end{aligned}$$

where m denotes the mass fraction and the subscripts "ft", "sk", "th", "pel" and "hat" indicate the foot, shank, thigh, pelvis and HAT segments, respectively, and the superscripts "sw" and "st" indicate swing and stance legs, respectively. Using Eq. (2) the accelerations of the COM of each segment can be expressed as

$$\begin{aligned}
{}^{\text{st}}\boldsymbol{A}_{\text{ft}} =& {}^{\text{st}}\boldsymbol{A}_{\text{ank}} + {}^{\text{st}}\mathbf{E}_{\text{ft}}(-\boldsymbol{r}_2),\\
{}^{\text{st}}\boldsymbol{A}_{\text{sk}} =& {}^{\text{st}}\boldsymbol{A}_{\text{ank}} + {}^{\text{st}}\mathbf{E}_{\text{sk}}(-\boldsymbol{r}_3),\\
{}^{\text{st}}\boldsymbol{A}_{\text{th}} =& {}^{\text{st}}\boldsymbol{A}_{\text{ank}} + {}^{\text{st}}\mathbf{E}_{\text{sk}}(-\boldsymbol{r}_3+\boldsymbol{r}_4) + {}^{\text{st}}\mathbf{E}_{\text{th}}(-\boldsymbol{r}_5),\\
\boldsymbol{A}_{\text{hat}} =& {}^{\text{st}}\boldsymbol{A}_{\text{ank}} + {}^{\text{st}}\mathbf{E}_{\text{sk}}(-\boldsymbol{r}_3+\boldsymbol{r}_4) + {}^{\text{st}}\mathbf{E}_{\text{th}}(-\boldsymbol{r}_5+\boldsymbol{r}_6)\\
&+ \mathbf{E}_{\text{pel}}(-\boldsymbol{r}_7) + \mathbf{E}_{\text{hat}}\boldsymbol{r}_8,\\
{}^{\text{sw}}\boldsymbol{A}_{\text{th}} =& {}^{\text{st}}\boldsymbol{A}_{\text{ank}} + {}^{\text{st}}\mathbf{E}_{\text{sk}}(-\boldsymbol{r}_3+\boldsymbol{r}_4) + {}^{\text{st}}\mathbf{E}_{\text{th}}(-\boldsymbol{r}_5+\boldsymbol{r}_6)\\
&+ \mathbf{E}_{\text{pel}}(-\boldsymbol{r}_7+\boldsymbol{r}_9) + {}^{\text{sw}}\mathbf{E}_{\text{th}}(-\boldsymbol{r}_{10}),\\
{}^{\text{sw}}\boldsymbol{A}_{\text{sk}} =& {}^{\text{st}}\boldsymbol{A}_{\text{ank}} + {}^{\text{st}}\mathbf{E}_{\text{sk}}(-\boldsymbol{r}_3+\boldsymbol{r}_4) + {}^{\text{st}}\mathbf{E}_{\text{th}}(-\boldsymbol{r}_5+\boldsymbol{r}_6)\\
&+ \mathbf{E}_{\text{pel}}(-\boldsymbol{r}_7+\boldsymbol{r}) + {}^{\text{sw}}\mathbf{E}_{\text{th}}(-\boldsymbol{r}_{10}+\boldsymbol{r}_{11})\\
&+ {}^{\text{sw}}\mathbf{E}_{\text{sk}}(-\boldsymbol{r}_{12}) \text{ and}\\
{}^{\text{sw}}\boldsymbol{A}_{\text{ft}} =& {}^{\text{st}}\boldsymbol{A}_{\text{ank}} + {}^{\text{st}}\mathbf{E}_{\text{sk}}(-\boldsymbol{r}_3+\boldsymbol{r}_4) + {}^{\text{st}}\mathbf{E}_{\text{th}}(-\boldsymbol{r}_5+\boldsymbol{r}_6)\\
&+ \mathbf{E}_{\text{pel}}(-\boldsymbol{r}_7+\boldsymbol{r}_9) + {}^{\text{sw}}\mathbf{E}_{\text{th}}(-\boldsymbol{r}_{10}+\boldsymbol{r}_{11})\\
&+ {}^{\text{sw}}\mathbf{E}_{\text{sk}}(-\boldsymbol{r}_{12}+\boldsymbol{r}_{13}) + {}^{\text{sw}}\mathbf{E}_{\text{ft}}(-\boldsymbol{r}_{14}). \qquad \text{(A3)}
\end{aligned}$$

Expressing all $\mathbf{E}\boldsymbol{r}$s in Eq. (A3) in column vector notation (Eq. 4) and using in Eq. (A2) gives

$$\begin{aligned}
\boldsymbol{A}_{\text{com}} =& {}^{\text{st}}\boldsymbol{A}_{\text{ank}} + k_1\begin{bmatrix} | \\ {}^{\text{st}}\mathbf{E}_{\text{ft}} \\ | \end{bmatrix}_{c2} + k_2\begin{bmatrix} | \\ {}^{\text{st}}\mathbf{E}_{\text{sk}} \\ | \end{bmatrix}_{c2}\\
&+ k_3\begin{bmatrix} | \\ {}^{\text{st}}\mathbf{E}_{\text{th}} \\ | \end{bmatrix}_{c2} + k_4\begin{bmatrix} | \\ \mathbf{E}_{\text{pel}} \\ | \end{bmatrix}_{c3} + k_5\begin{bmatrix} | \\ \mathbf{E}_{\text{hat}} \\ | \end{bmatrix}_{c2}\\
&+ k_6\begin{bmatrix} | \\ {}^{\text{sw}}\mathbf{E}_{\text{th}} \\ | \end{bmatrix}_{c2} + k_7\begin{bmatrix} | \\ {}^{\text{sw}}\mathbf{E}_{\text{sk}} \\ | \end{bmatrix}_{c2} + k_8\begin{bmatrix} | \\ {}^{\text{sw}}\mathbf{E}_{\text{ft}} \\ | \end{bmatrix}_{c2} \qquad \text{(A4)}
\end{aligned}$$

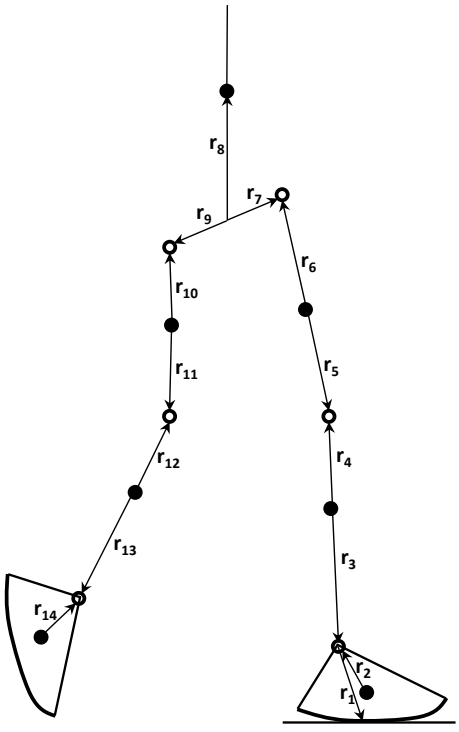

Figure A1. Link segment model showing the position vectors in each segment.

where

$$\begin{aligned}
k_1 &= -{}^{\text{st}}m_{\text{ft}}r_{2y},\\
k_2 &= -\left(1-{}^{\text{st}}m_{\text{ft}}\right)r_{3y} + \left(1-{}^{\text{st}}m_{\text{ft}}-{}^{\text{st}}m_{\text{sk}}\right)r_{4y},\\
k_3 &= -\left(1-{}^{\text{st}}m_{\text{ft}}-{}^{\text{st}}m_{\text{sk}}\right)r_{5y} + \left(1-{}^{\text{st}}m_{\text{ft}}-{}^{\text{st}}m_{\text{sk}}-{}^{\text{st}}m_{\text{th}}\right)r_{6y},\\
k_4 &= -\left(1-{}^{\text{st}}m_{\text{ft}}-{}^{\text{st}}m_{\text{sk}}-{}^{\text{st}}m_{\text{th}}\right)r_{7z} + \left({}^{\text{sw}}m_{\text{ft}}+{}^{\text{sw}}m_{\text{sk}}+{}^{\text{sw}}m_{\text{th}}\right)r_{9z},\\
k_5 &= m_{\text{hat}}r_{8y},\\
k_6 &= -\left({}^{\text{sw}}m_{\text{ft}}+{}^{\text{sw}}m_{\text{sk}}+{}^{\text{sw}}m_{\text{th}}\right)r_{10y} + \left({}^{\text{sw}}m_{\text{ft}}+{}^{\text{sw}}m_{\text{sk}}\right)r_{11y},\\
k_7 &= -\left({}^{\text{sw}}m_{\text{ft}}+{}^{\text{sw}}m_{\text{sk}}\right)r_{12y} + {}^{\text{sw}}m_{\text{ft}}r_{13y} \text{ and}\\
k_8 &= -{}^{\text{sw}}m_{\text{ft}}r_{14y}. \qquad \text{(A5)}
\end{aligned}$$

Each $\mathbf{E}$ is a function of the kinematics of the corresponding segment. The terms ${}^{\text{st}}\boldsymbol{A}_{\text{ank}}$ and ${}^{\text{st}}\mathbf{E}_{\text{ft}}$ are functions of foot kinematics when the FROS model is used. However, when AFROS is used (since $\theta_1 = \theta_2 - \theta_{\text{ank}}$), ${}^{\text{st}}\boldsymbol{A}_{\text{ank}}$ and ${}^{\text{st}}\mathbf{E}_{\text{ft}}$ are functions of shank kinematics. Using Eq. (A2) in Newton's equation (Eq. 6) we get

$$\begin{aligned}
\boldsymbol{GRF} &= M\boldsymbol{A}_{\text{com}} - M\boldsymbol{g}\\
&= M\,{}^{\text{st}}\boldsymbol{A}_{\text{ank}} + M\sum k\begin{bmatrix} | \\ \mathbf{E} \\ | \end{bmatrix} - M\boldsymbol{g}. \qquad \text{(A6)}
\end{aligned}$$

Therefore, GRF is given by

$$\begin{aligned}
\boldsymbol{GRF} =& {}^{\text{st}}\boldsymbol{R}_{\text{ft}} + {}^{\text{st}}\boldsymbol{R}_{\text{sk}} + {}^{\text{st}}\boldsymbol{R}_{\text{th}} + \boldsymbol{R}_{\text{pel}}\\
&+ \boldsymbol{R}_{\text{hat}} + {}^{\text{sw}}\boldsymbol{R}_{\text{th}} + {}^{\text{sw}}\boldsymbol{R}_{\text{sk}} + {}^{\text{sw}}\boldsymbol{R}_{\text{ft}} \qquad \text{(A7)}
\end{aligned}$$

where

$$ {}^{\mathrm{st}}\boldsymbol{R}_{\mathrm{ft}} = M\,{}^{\mathrm{st}}\boldsymbol{A}_{\mathrm{ank}} + Mk_1 \begin{bmatrix} | \\ {}^{\mathrm{st}}\mathbf{E}_{\mathrm{ft}} \\ | \end{bmatrix}_{c2} - {}^{\mathrm{st}}m_{\mathrm{ft}} M\boldsymbol{g}, \tag{A8} $$

$$ {}^{\mathrm{st}}\boldsymbol{R}_{\mathrm{sk}} = Mk_2 \begin{bmatrix} | \\ {}^{\mathrm{st}}\mathbf{E}_{\mathrm{sk}} \\ | \end{bmatrix}_{c2} - {}^{\mathrm{st}}m_{\mathrm{sk}} M\boldsymbol{g}, \tag{A9} $$

$$ {}^{\mathrm{st}}\boldsymbol{R}_{\mathrm{th}} = Mk_3 \begin{bmatrix} | \\ {}^{\mathrm{st}}\mathbf{E}_{\mathrm{th}} \\ | \end{bmatrix}_{c2} - {}^{\mathrm{st}}m_{\mathrm{th}} M\boldsymbol{g}, \tag{A10} $$

$$ \boldsymbol{R}_{\mathrm{pel}} = Mk_4 \begin{bmatrix} | \\ \mathbf{E}_{\mathrm{pel}} \\ | \end{bmatrix}_{c3}, \tag{A11} $$

$$ \boldsymbol{R}_{\mathrm{hat}} = Mk_5 \begin{bmatrix} | \\ \mathbf{E}_{\mathrm{hat}} \\ | \end{bmatrix}_{c2} - m_{\mathrm{hat}} M\boldsymbol{g}, \tag{A12} $$

$$ {}^{\mathrm{sw}}\boldsymbol{R}_{\mathrm{th}} = Mk_6 \begin{bmatrix} | \\ {}^{\mathrm{sw}}\mathbf{E}_{\mathrm{th}} \\ | \end{bmatrix}_{c2} - {}^{\mathrm{sw}}m_{\mathrm{th}} M\boldsymbol{g}, \tag{A13} $$

$$ {}^{\mathrm{sw}}\boldsymbol{R}_{\mathrm{sk}} = Mk_7 \begin{bmatrix} | \\ {}^{\mathrm{sw}}\mathbf{E}_{\mathrm{sk}} \\ | \end{bmatrix}_{c2} - {}^{\mathrm{sw}}m_{\mathrm{sk}} M\boldsymbol{g} \text{ and} \tag{A14} $$

$$ {}^{\mathrm{sw}}\boldsymbol{R}_{\mathrm{ft}} = Mk_8 \begin{bmatrix} | \\ {}^{\mathrm{sw}}\mathbf{E}_{\mathrm{ft}} \\ | \end{bmatrix}_{c2} - {}^{\mathrm{sw}}m_{\mathrm{ft}} M\boldsymbol{g}. \tag{A15} $$

The general form of the column vectors in the above equations are given below. The second column vector of the **E** matrix for the foot, shank and thigh segments is given by

$$ \begin{bmatrix} | \\ {}^{q}\mathbf{E}_{p} \\ | \end{bmatrix}_{c2} = \begin{bmatrix} \omega_z^2 S_z - \alpha_z C_x C_z + \omega_x \omega_z S_z C_z \\ -S_z \alpha_z - \left(\omega_x^2 + \omega_z^2\right) C_x C_z - \alpha_x S_x C_z \\ -\omega_x \omega_z S_z + \alpha_x C_x C_z - \omega_x^2 S_x C_z \end{bmatrix} \tag{A16} $$

where

$x = 4$ and $z = 1$ for $q = \mathrm{st}$ and $p = \mathrm{ft}$,
$x = 4$ and $z = 2$ for $q = \mathrm{st}$ and $p = \mathrm{sk}$,
$x = 4$ and $z = 3$ for $q = \mathrm{st}$ and $p = \mathrm{th}$,
$x = 8$ and $z = 9$ for $q = \mathrm{sw}$ and $p = \mathrm{th}$,
$x = 8$ and $z = 10$ for $q = \mathrm{sw}$ and $p = \mathrm{sk}$,
$x = 8$ and $z = 11$ for $q = \mathrm{sw}$ and $p = \mathrm{ft}$,
$\theta_x = 0$ and $z = 7$ for $p = \mathrm{hat}$,

$S_i = \sin\theta_i$, $C_i = \cos\theta_i$, $\omega_i = \dot{\theta}_i$ and $\alpha_i = \ddot{\theta}_i$. The first column vector of the ${}^{\mathrm{st}}\mathbf{E}_{\mathrm{ft}}$ matrix for the foot segment is given by

$$ \begin{bmatrix} | \\ {}^{\mathrm{st}}\mathbf{E}_{\mathrm{ft}} \\ | \end{bmatrix}_{c1} = \begin{bmatrix} \omega_1^2 C_1 - \alpha_1 C_4 S_1 + \omega_4 \omega_1 S_1 S_4 \\ C_1 \alpha_1 - \left(\omega_1^2 + \omega_4^2\right) C_4 S_1 - \alpha_4 S_4 S_1 \\ -\omega_4 \omega_1 C_1 + \alpha_4 C_4 S_1 - \omega_4^2 S_4 S_1 \end{bmatrix} \tag{A17} $$

and third column vector of $\mathbf{E}_{\mathrm{pel}}$ is given by

$$ \begin{bmatrix} | \\ \mathbf{E}_{\mathrm{pel}} \\ | \end{bmatrix}_{c3} = \begin{bmatrix} -\omega_6^2 S_6 - \omega_5 \omega_6 S_5 C_6 + \alpha_6 C_5 C_6 \\ \omega_5 \omega_6 S_6 + \omega_5^2 S_5 C_6 - \alpha_5 C_5 C_6 \\ -\alpha_6 S_6 - \alpha_5 S_5 C_6 - \left(\omega_5^2 + \omega_6^2\right) C_5 C_6 \end{bmatrix}. \tag{A18} $$

Appendix B: Rolling foot kinematics

In the case of the rolling foot (analogous to the rolling coin problem (Greenwood, 1988)), the acceleration of the contact point, center of ROS and the ankle of the rolling foot are determined as

$$ \begin{aligned} \boldsymbol{A}_{\mathrm{cp}} &= (\omega_z C_4)^2 R_{\mathrm{roll}} \hat{u}, \\ \boldsymbol{A}_{\mathrm{o}} &= \boldsymbol{A}_{\mathrm{cp}} + \left({}^{\mathrm{st}}\tilde{\alpha}_{\mathrm{p}} + {}^{\mathrm{st}}\tilde{\omega}_{\mathrm{p}}\,{}^{\mathrm{st}}\tilde{\omega}_{\mathrm{p}}\right) R_{\mathrm{roll}} \hat{u} \text{ and} \\ \boldsymbol{A}_{\mathrm{ank}} &= \boldsymbol{A}_{\mathrm{o}} + {}^{\mathrm{st}}\mathbf{E}_{\mathrm{p}} \boldsymbol{s} \end{aligned} \tag{B1} $$

where $\hat{u} = (0,\ C_4,\ S_4)'$ and R_{roll} is the radius of the roll-over shape, $p = \mathrm{ft}$ and $z = 1$ for FROS, $p = \mathrm{sk}$ and $z = 2$ for AFROS and $\boldsymbol{s}$ is the vector from the center of ROS to the ankle.

Edited by: J. Schmiedeler
Reviewed by: two anonymous referees

References

Anderson, F. C. and Pandy, M. G.: Dynamic Optimization of Human Walking, J. Biomech. Eng., 123, 381–390, 2001.

Firmani, F. and Park, E. J.: Theoretical Analysis of the State of Balance in Bipedal Walking, J. Biomech. Eng., 135, 041003, doi:10.1115/1.4023698, 2013.

Greenwood, D. T.: Principles of Dynamics, Prentice Hall, New Jersey, 1988.

Hansen, A. H. and Childress, D. S.: Effects of shoe heel height on biologic roll-over characteristics during walking, J. Rehab. Res. Develop., 41, 547–554, 2004.

Hansen, A. H. and Childress, D. S.: Effects of adding weight to the torso on roll-over characteristics of walking, J. Rehab. Res. Develop., 42, 381–390, 2005.

Hansen, A. H., Childress, D. S., and Knox, E. H.: Prosthetic foot roll-over shapes with implications for alignment of trans-tibial prostheses, Prosthet. Orthot. Int., 24, 205–215, 2000.

Hansen, A. H., Childress, D. S., and Knox, E. H.: Roll-over shapes of human locomotor systems: effects of walking speed, Clin. Biomech., 19, 407–414, 2004.

Hatze, H.: A comprehensive model for human motion simulation and its application to the take-off phase of the long jump, J. Biomech., 14, 135–142, 1981.

Herr, H. and Popovic, M.: Angular momentum in human walking, J. Exp. Biol., 211, 467–81, 2008.

Inman, V. T., Ralston, H. J., and Todd, F.: Human Walking, Williams & Wilkins, Baltimore, London, 1981.

Ju, M. S. and Mansour, J. M.: Simulation of the double limb support phase of human gait, J. Biomech. Eng., 110, 223–229, 1988.

Kane, T. R., Likins, P. W., and Levinson, D. A.: Spacecraft Dynamics, McGraw Hill, Ithaca, New York, 1983.

Koopman, B., Grootenboer, H. J., and deJongh, H. J.: An inverse dynamics model for the analysis, reconstruction and prediction of bipedal walking, J. Biomech., 28, 1369–1376, 1995.

Kuo, A. D.: The six determinants of gait and the inverted pendulum analogy: A dynamic walking perspective, Human Move. Sci., 26, 617–656, 2007.

Martin, A. E. and Schmiedeler, J. P.: Predicting human walking gaits with a simple planar model, J. Biomech., 47, 1416–1421, 2014.

Mccaw, S. T. and Devitat, P.: Errors in alignment of center of pressure and foot coordinates affect predicted lower extremity torques, J. Biomech., 28, 985–988, 1995.

McGeer, T.: Passive Dynamic Walking, Int. J. Robot. Res., 9, 62–82, 1990.

Mochon, S. and McMahon, T. A.: Ballistic walking: an improved model, Math. Biosci., 52, 241–260, 1980.

Oh, S. E., Choi, A., and Hwan, J.: Prediction of ground reaction forces during gait based on kinematics and a neural network model, J. Biomech., 46, 2372–2380, 2013.

Onyshko, S. and Winter, D. A.: A mathematical model for the dynamics of human locomotion, J. Biomech., 13, 361–368, 1980.

Pàmies-Vilà, R., Font-Llagunes, J. M., Cuadrado, J., and Alonso, F. J.: Analysis of different uncertainties in the inverse dynamic analysis of human gait, Mech. Mach. Theory, 58, 153–164, 2012.

Pandy, M. G. and Berme, N.: Synthesis of human walking: A planar model for single support, J. Biomech., 21, 1053–1060, 1988.

Pandy, M. G. and Berme, N.: Quantitative assessment of gait determinants during single stance via a three-dimensional model – Part 2. Pathological gait, J. Biomech., 22, 725–733, 1989a.

Pandy, M. G. and Berme, N.: Quantitative assessment of gait determinants during single stance via a three-dimensional model – Part 1. Normal gait, J. Biomech., 22, 717–724, 1989b.

Pearsall, D. J. and Costigan, P. A.: The effect of segment parameter error on gait analysis results, Gait Posture, 9, 173–83, 1999.

Perry, J.: Gait Analysis Normal and Pathological Function, SLACK Inc., Thorofare, New Jersey, 1992.

Pillet, H., Bonnet, X., Lavaste, F., and Skalli, W.: Evaluation of force plate-less estimation of the trajectory of the centre of pressure during gait. Comparison of two anthropometric models, Gait Posture, 31, 147–152, 2010.

Rao, G., Amarantini, D., Berton, E., and Favier, D.: Influence of body segments' parameters estimation models on inverse dynamics solutions during gait, J. Biomech. 39, 1531–1536, 2006.

Reinbolt, J. A., Haftka, R. T., Chmielewski, T. L., and Fregly, B. J.: Are patient-specific joint and inertial parameters necessary for accurate inverse dynamics analyses of gait?, IEEE T. Biomed. Eng., 54, 782–793, 2007.

Ren, L., Jones, R. K., and Howard, D.: Predictive modelling of human walking over a complete gait cycle, J. Biomech., 40, 1567–1574, 2007.

Riemer, R., Hsiao-Wecksler, E. T., and Zhang, X.: Uncertainties in inverse dynamics solutions: a comprehensive analysis and an application to gait, Gait Posture, 27, 578–588, 2008.

Saunders, J. B., Inman, V. T., and Eberhart, H. D.: The major determinants in normal and pathological gait, J. Bone Joint Surge., 35A, 543–558, 1953.

Selles, R. W., Bussmann, J. B., Wagenaar, R. C., and Stam, H. J.: Comparing predictive validity of four ballistic swing phase models of human walking, J. Biomech., 34, 1171–1177, 2001.

Shabana, A. A.: Computational Dynamics, Wiley, New York, 2010.

Silva, M. P. and Ambrosio, J. A. C.: Sensitivity of the results produced by the inverse dynamic analysis of a human stride to perturbed input data, Gait Posture, 19, 35–49, 2004.

Srinivasan, S., Raptis, I. A., and Westervelt, E. R.: Low-dimensional sagittal plane model of normal human walking, J. Biomech. Eng. – T. ASME, 130, 051017, doi:10.1115/1.2970058, 2008.

Srinivasan, S., Westervelt, E. R., and Hansen, A. H.: A Low-Dimensional Sagittal-Plane Forward-Dynamic Model for Asymmetric Gait and Its Application to Study the Gait of Transtibial Prosthesis Users, J. Biomech. Eng – T. ASME, 131, 031003, doi:10.1115/1.3002757, 2009.

Thornton-Trump, A. and Daher, R.: The prediction of reaction forces from gait data, J. Biomech., 8, 173–178, 1975.

Vanderpool, M. T., Collins, S. H., and Kuo, A. D.: Ankle fixation need not increase the energetic cost of human walking, Gait Posture, 28, 427–433, 2008.

Wang, C. C. and Hansen, A. H.: Response of able-bodied persons to changes in shoe rocker radius during walking: Changes in ankle kinematics to maintain a consistent roll-over shape, J. Biomech., 43, 2288–2293, 2010.

Winiarski, S. and Rutkowska-Kucharska, A.: Estimated ground reaction force in normal and pathological gait, Acta Bioeng. Biomech., 11, 53–60, 2009.

Winter, D. A.: The biomechanics and motor control of human gait: normal, elderly and pathological, University of Waterloo Press, Waterloo, 2005.

Zarrugh, M.: Kinematic prediction of intersegment loads and power at the joints of the leg in walking, J. Biomech., 14, 713–725, 1981.